Experiments on the Scaling of Tip Vortex Cavitation Inception for Elliptical Hydrofoils

by　Takayuki Mori*, *Member*　Kenshiro Takahashi*, *Member*
Matthew Khoo**　James Venning***

Key Words: *Tip Vortex Cavitation, Cavitation Inception.*

1. INTRODUCTION

Cavitation has been a major concern to naval engineers as it induces hydrodynamic noise and vibration of marine propellers in both naval and civilian ships. On typical marine propellers, cavitation begins in tip vortices that trail from the tip of the blades. However, model-scale evaluation of full-scale tip vortex cavitation inception is very difficult due to its strong dependency on nuclei population.

Reynolds number dependence of tip vortex cavitation inception has been studied by many authors [1)-5)]. McCormick [1)] reported that cavitation inception number, σ_i, varied with a power of Reynolds number, Re^n. Although McCormick reported the index n to be 0.35, different values of n were proposed by other researchers.

In the present study, Reynolds number dependence of the tip vortex cavitation inception was investigated for elliptical hydrofoils using cavitation tunnels in Japan and Australia. Inception and dynamics of the cavitating flows were observed using a high speed camera. Nuclei distributions were measured by a Cavitation Susceptibility Meter (CSM).

2. EXPERIMENTAL SETUP

2. 1 Cavitation Tunnels

The research program was carried out in cavitation tunnels at the Naval Systems Research Center (NSRC) and the University of Tasmania's Australian Maritime College (AMC). The NSRC cavitation tunnel, the Flow Noise Simulator (FNS), is a large and quiet tunnel suitable for tests with large scale models. The dimensions of the test section are 2m (Width) × 2m (Height) × 10m (Length). The AMC cavitation tunnel is a medium-sized test facility and has excellent capabilities for the study of nuclei effects on cavitation. The dimensions of the test section are 0.6m (Width) × 0.6m (Height) × 2.6m (Length). The tunnel has a large downstream tank and resorber tank to prevent recirculation of microbubbles. Further details of the cavitation tunnels can be found in ref. [6)] and [7)].

2. 2 Hydrofoils

Three hydrofoils with different chord lengths were used in the present study. The hydrofoils are elliptical planform of aspect ratio of 3, and a NACA 0012 cross-section. The hydrofoils were manufactured in Australia. The chord lengths of the large, medium and small hydrofoils are 500 mm, 150 mm and 75 mm, respectively (Figure 1). In the FNS, the large and medium hydrofoils were attached to the top wall of the test section. The streamwise position of the hydrofoil tip was 3.6m from the test section inlet. The momentum thickness of the top wall boundary layer at that location was estimated to be 9mm from LDV measurements. In the case of the small hydrofoil, the spanwise length of the hydrofoil was similar to the boundary layer thickness of the test section. Hence, a ground plate was used for the small hydrofoil to reduce influence of the tunnel boundary layer. A side window of the test section was used for the small hydrofoil test, and the vertical position of the hydrofoil was 450 mm from the test section ceiling. In the AMC cavitation tunnel, the medium and small hydrofoils were attached to the top wall of the test section.

2. 3 Measuring Instruments

In both water tunnels, inception of tip vortex cavitation was observed acoustically and visually. In the FNS, acoustic noise was measured using a piezoelectric hydrophone (Brüel & Kjær, BK-8104) located in a water tank attached to the bottom wall of the tunnel test section. The hydrophone was paired with a voltage amplifier designed for the FNS. In the AMC cavitation tunnel, acoustic noise was measured using a piezoelectric hydrophone (Brüel & Kjær, BK-8103) mounted in the ceiling of the test section. The acoustic signals were amplified with a conditioning amplifier (Brüel & Kjær, BK-2692).

Cavitation observation was made using a high-speed video system. (Vision Research, Phantom 5.1) in the FNS. The frame rate of the high-speed video observation was 2000 frame per second (fps) or 3000 fps. In the AMC cavitation tunnel, cavitation photographs were taken using a high-resolution DSLR camera (Nikon D850).

Nuclei population of the cavitation tunnels were measured using Cavitation Susceptibility Meters (CSM) provided by each participant. The CSM has a piezoceramic sensor mounted near the centerbody venturi and is used to measure the nuclei bubble concentration distribution in the tunnel water[8),9)]. In both facilities, tunnel water was sampled from the test section through a streamlined sampling probe. In the FNS, the probe was mounted to a side window located 4m downstream of the test section inlet.

2. 4 Test Procedure

In the FNS, inception tests were carried out using a fixed procedure as the nuclei population of the tunnel water strongly depends on the tunnel's operational history[8)]. At the beginning of each inception test, the static pressure at the tunnel

* Naval Systems Research Center, ATLA, Ministry of Defense
** Maritime Division, Defence Science and Technology Group, Australia
*** Cavitation Research Laboratory, University of Tasmania, Australia
Received　6th March 2020
Published　18th May 2020
Read at the spring meeting 2020.

centerline was kept at 200 kPa for 10 minutes to minimize the population of free gas bubbles and the influence of tunnel operation history. Nuclei measurements were carried out when tip vortex cavitation inception was detected. In the AMC tunnel, influence of tunnel operating history on the nuclei population is less significant than that in the FNS. In both cavitation tunnels, the static pressure was reduced in 5kPa intervals at the designated free stream velocity, U_0. For several test conditions, acoustic signals were recorded simultaneously with high-speed video observations.

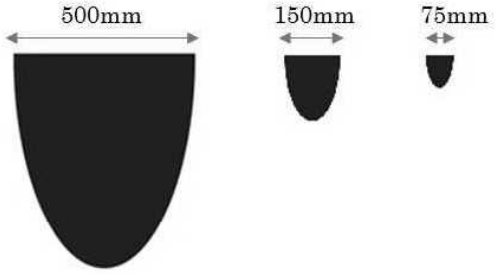

Fig. 1 Planform of the large (left), medium (middle) and small (right) hydrofoil models

3. NUCLEI POPULATION

In the FNS, there is a critical pressure, p_{crit}, below which the nuclei population increases significantly[5),8)]. For cavitation inception measurement, the focus of nuclei measurement is to determine whether the inception pressure is lower than the critical pressure.

Figure 2 shows representative examples of nuclei distributions measured during the large hydrofoil test. Here, p_{th} and p_v denote static pressure at the venturi throat and the vapor pressure, respectively. The reference pressure, p, is defined as the static pressure at the centerline of the test section.

The result shows an increase of nuclei population at p < 50kPa which indicates that the critical pressure in the experiment was p~50kPa. In the figure, high nuclei population is observed at $-(p_{th}-p_v)$ ~ 40kPa at higher pressure of 88kPa and 8m/s in the test section. However, this result was regarded as a measurement artifact because such an increase in nuclei population was not observed in other measurements at this range of static pressures. With the exception of these conditions, results for p=200kPa and 88kPa show good agreement. Hereafter, this distribution is termed the baseline condition of the nuclei population.

4. TIP VORTEX CAVITATION INCEPTION

As reported in prior studies[2),3),5)], different types of cavitation phenomena were observed in the period of cavitation inception. Typically, as the static pressure decreases from non-cavitating condition, single and intermittent cavitation bubbles are initially observed in the low pressure region around the tip vortex. In the present study, this initial phase of the inception is referred to as "intermittent". As the static pressure is decreased, the cavitation bubbles become persistent in the same streamwise position for several seconds. The persisting cavitation bubbles are referred to as "persistent". As the static pressure is further decreased, the persistent cavitation bubble becomes more stable and overlaps with the hydrofoil tip. The stable behavior is referred to as "overlapped". Finally, at sufficiently low static pressure, sheet cavitation occurs near the surface of the hydrofoil tip.

In the present study, the incipient cavitation number, σ_i, ($\sigma_i=(p_i-p_v)/1/2\rho U_0^2$) was defined as a cavitation number in which a continuous vortex tube has overlapped with the tip of the hydrofoil. Here p_i denotes static pressure at inception. For inception test, static pressure at the hydrofoil tip was used to characterize σ_i.

Inception cavitation numbers in the FNS are shown in fig.4 for α=4°,6°, 8° and 10° as a function of Reynolds number based on hydrofoil chord length at the root, Re_C. Here, filled and open symbols correspond to results obtained above and below the critical pressure, p_{crit}, respectively. In the case of the

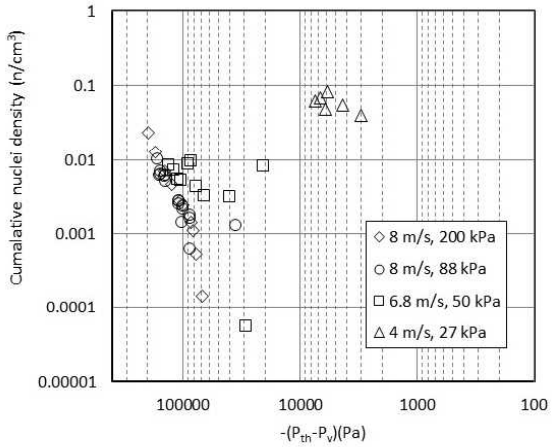

Fig. 2 Nuclei distribution in the FNS for various test section velocities and static pressures

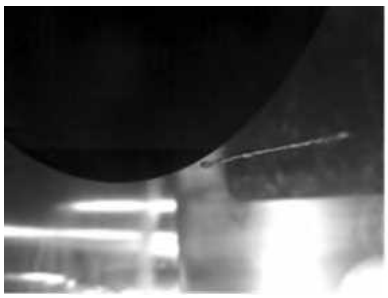

(a) Persistent cavitation bubble

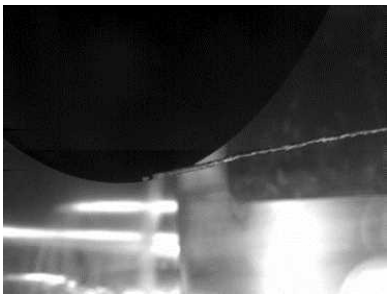

(b) Overlapped with hydrofoil

Fig. 3 Photographs of tip vortex cavitation during its development

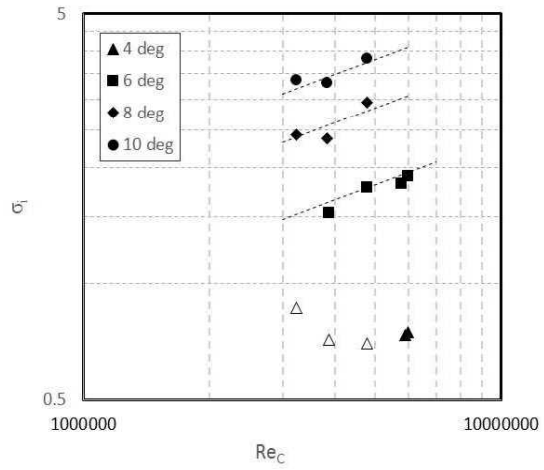

(a) Large hydrofoil

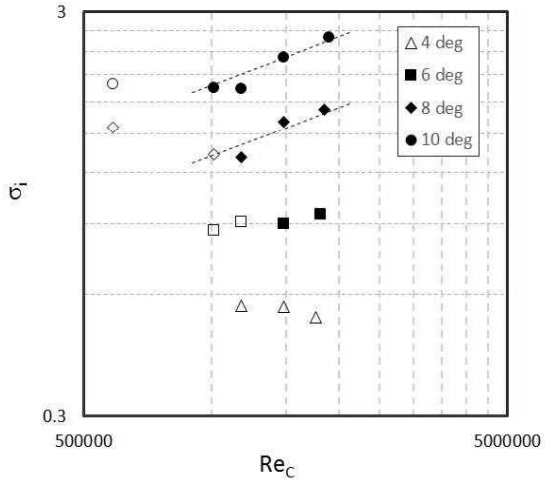

(b) Medium hydrofoil

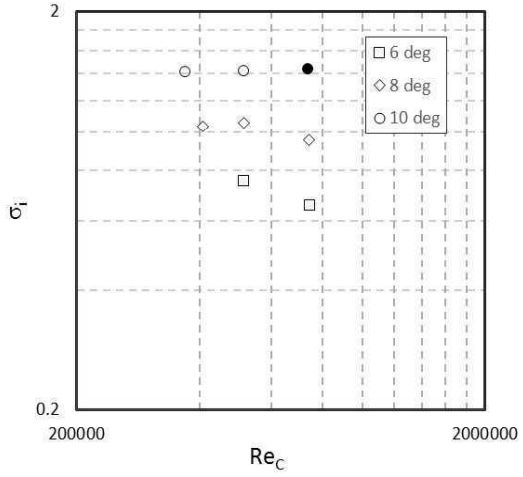

(c) Small hydrofoil

Fig. 4 Inception cavitation number, σ_i, as a function of Re_C in the FNS. The filled and open symbols correspond to results obtained at above and below the critical pressure, respectively. The dashed lines represent $Re_C^{0.4}$.

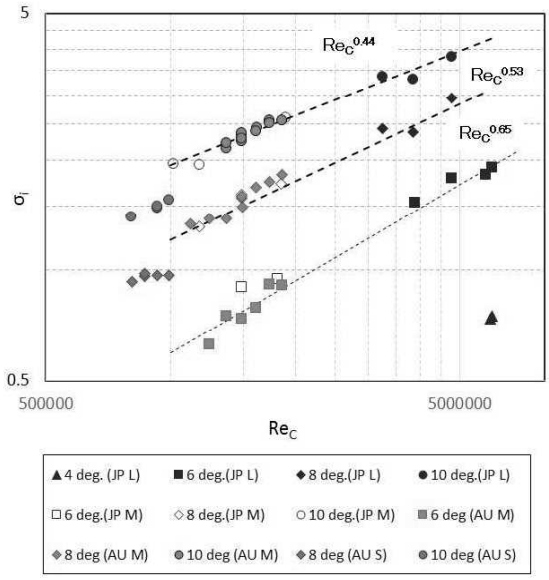

Fig. 5 Summary of tip vortex cavitation (TVC) inception indices for the three hydrofoils in the FNS and the AMC cavitation tunnel. In the legend, L, M and S denote large, medium and small hydrofoils, respectively. The lines represent the power law slopes.

small hydrofoil, cavitation inception occurred at static pressures lower than the critical pressure except for the case of $\alpha=10°$ and $Re_C=7.4\times10^5$. For the large and medium hydrofoils, inception cavitation numbers obtained at $p > p_{crit}$ show obvious Reynolds number dependency. Observed Reynolds number dependence of σ_i shows relatively good agreement with a power law slope of $Re_C^{0.4}$. On the other hand, results obtained at $p < p_{crit}$ do not show observable Reynolds number dependency. This is, at least partially, due to significant variation of nuclei population in the range of $p < p_{crit}$.

Figure 5 summarizes inception cavitation number, σ_i, as a function of Re_C. Results measured at the two cavitation tunnels are presented. Since the plot is intended to compare Reynolds number dependence in the two cavitation tunnels, results obtained at the baseline nuclei conditions are shown for the FNS. Results for the small hydrofoil were not shown as the test was carried out at a low pressure range below the critical pressure. For the AMC cavitation tunnel, all results plotted in the figure were obtained at baseline nuclei condition. Baseline nuclei conditions have previously been found to be similar between the two cavitation tunnels[8].

For the medium hydrofoil, Reynolds number dependence of σ_i shows good agreement between the FNS and AMC Tunnel. Considering the difference of the tunnel characteristics, this agreement is much better than expected. Combined with results for the large hydrofoil, the power law index is 0.44 for $\alpha=10°$, which is close to the value of 0.4 obtained using the empirical model for turbulent boundary layer thickness over a flat plate[10),11)]. At lower α, better collapses are observed for power indices of 0.53 and 0.65, which are larger than the typical values of prior studies [1)-4)]. Although individual data shows some scatter, present inception results are in relatively good agreement with prior studies. It should be noted that

relatively low Reynolds numbers, particularly near the tips of the small and medium hydrofoils, may result in laminar boundary layers which could influence vortex characteristics and Reynolds number scaling parameters. Further investigation is recommended to clarify the relationship between the boundary layer and tip vortex characteristics.

5. TIP VORTEX CAVITATION NOISE

Figure 6 shows a time series of acoustic signal emitted from a growing tip vortex cavitation bubble. Photographs taken at the growth (T=0.0075s) and persistent (T=0.033s) phases are also shown. At T=0.0075s, the cylindrical cavitation bubble has a head and neck. While the cylindrical bubble grows explosively, the location of the "bubble head" does not show significant time-variation. The head of the bubble gradually moves to the hydrofoil tip and the bubble becomes persistent when its head overlaps with the hydrofoil tip. The amplitude of the acoustic signal significantly increases in the period of the bubble explosion. Once the persistent cavitation bubble is formed, the amplitude of the acoustic signal decreases significantly.

The amplitude of acoustic pulses from individual intermittent cavitation bubbles are shown in fig.7 as a function static pressure at the centerline of the test section. Although the sample number of the measurement is not large, the results show a clear trend. The amplitude of the acoustic pulse tends to be larger for the large hydrofoil than the medium hydrofoil. The amplitude of the acoustic pulse tends to increase with decreasing static pressure for a given test section velocity.

Figure 8 presents the dominant frequency of the acoustic pulse from individual intermittent bubbles. The dominant frequency tends to be higher for the medium hydrofoil than the large hydrofoil. As the static pressure decreases, the dominant frequency tends to decrease for a given test section velocity.

6. CONCLUSION

Inception of tip vortex cavitation was investigated for elliptical hydrofoils with three different chord lengths using cavitation tunnels in Japan and Australia. Nuclei characteristics of the tunnel water were measured during the inception tests.

At inception, different types of cavitation phenomena were observed. As the static pressure decreases from the non-cavitating condition, single and intermittent cavitation bubbles were initially observed in the low pressure region around the tip vortex. The cavitation bubbles became persistent and overlapped with the tip as the static pressure further decreased.

Reynolds number dependency of the cavitation inception was measured for α=4°, 6°, 8° and 10°. For scaling, cavitation inception was defined as the formation of a cavity which overlapped with the hydrofoil tip. When the tunnel nuclei population remains at the baseline condition, Reynolds number dependence of inception cavitation number, σ_i, was clearly observed in both cavitation tunnels. At α=10°, Reynolds number dependence of inception cavitation number σ_i showed relatively good agreement with a power law slope of $Rec^{0.4}$. The power law index of the Reynolds number scaling increased as α is decreased.

Large amplitude acoustic pulses were observed during the growth phase of cavitation bubbles. The amplitude and dominant frequency of the acoustic pulse showed strong dependence on hydrofoil size and tunnel static pressure. The amplitudes of acoustic pulses emitted due to cavitation about the larger hydrofoil tended to be higher than those from the medium hydrofoil. The dominant frequency of the acoustic pulse decreased with decreasing tunnel static pressure.

ACKNOWLEDGMENT

The authors acknowledge the support of the University of Tasmania, the Defence Science and Technology Group and the Acquisition, Technology & Logistics Agency. We thank AMC technical officers, Mr Robert Wrigley and Mr Steven Kent, and Mr. Kenji Naganuma of NSRC for providing technical assistance with test facility configuration and operation. We are also extremely grateful to Dr. Dev Ranmuthugala of the Defence Science and Technology Group and Professor Paul Brandner of the University of Tasmania for their helpful insight and advice.

REFERENCES

1) B. W. McCormick: On cavitation produced by a vortex trailing from a lifting surface, Transaction of the ASME, J. Basic Engineering, Vol.84, No.3, pp.369-370, 1962

2) H. Higuchi, R. E. A. Arndt and M. F. Rogers, "Characteristics of tip vortex cavitation noise", Trans. ASME J. Fluids Eng., vol. 111, pp. 495-501, 1989

3) L. Briancon-Marjolet, and L. Merle, "Inception, development and noise of a tip vortex cavitation", Proceedings of 21st Symposium on Naval Hydrodynamics, Trondheim, Norway, pp.851-864, 1996

4) Y. T. Shen, S. Jessup, and S. Gowing, "The tip vortex cavitation scaling for high Reynolds number application", Proceedings of 4th ASME-JSME Fluids Engineering Division Joint Meeting, pp. 233-239, 2001

5) S. Nagaya, R. Kimoto, K. Naganuma and T. Mori: Observation and scaling of tip vortex cavitation on elliptical hydrofoils, Proceedings of ASME-JSME-KSME Joint Fluids Engineering Conference, pp. 225-230, 2011

6) T. Mori, K. Naganuma, R. Kimoto, R. Yakushiji and S. Nagaya: Hydrodynamic and hydroacoustic characteristics of the Flow Noise Simulator, Proceedings of 5th ASME-JSME Joint Fluids Engineering Conference, pp. 121-127, 2007.

7) P. Brandner, Y. Lecoffre and G. Walker: Design consideration in the development of a modern cavitation tunnel, Proceedings of 16th Australian Fluid Mechanics Conference, pp.630-637, 2007.

8) M. T. Khoo, J. A. Venning, B. W. Pearce, K. Takahashi, T. Mori, and P. A. Brandner. "Natural nuclei population dynamics in cavitation tunnels." Experiments in Fluids, Vol 61, 34, 2020

9) J. A. Venning, M. T. Khoo, B. W. Pearce, and P. A. Brandner. "Background nuclei measurements and implications for cavitation inception in hydrodynamic test facilities." Experiments in Fluids, Vol 59, 71, 2018

10) D. Fruman and C. Dugue. "Tip vortex roll-up and cavitation". Proceedings of 19th Symposium on Naval Hydrodynamics, pp. 633-654, 1994

11) H. Schlichting and K. Gersten. "Boundary-layer theory", Springer, 2016.

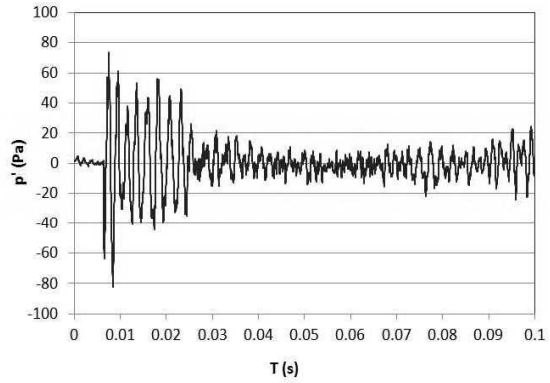

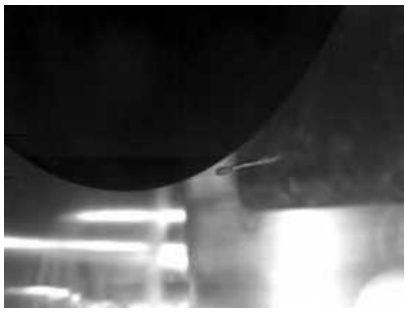

T=0.0075 s

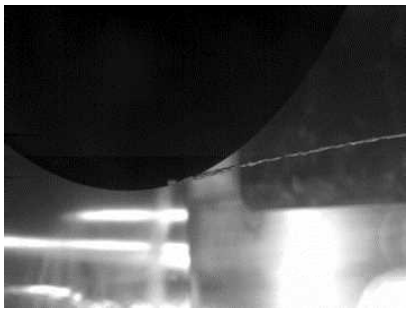

T=0.033 s

Fig. 6 Acoustic signal emitted during the formation of a persistent tip vortex cavity. Photographs taken at the growth and persistent phases are also shown.

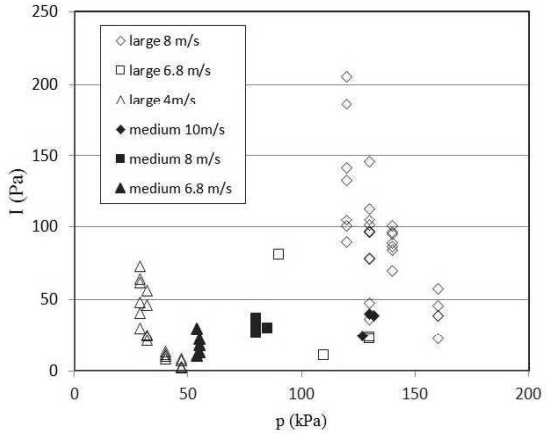

Fig. 7 Amplitude of the acoustic pulse, I, as a function of the test section static pressure

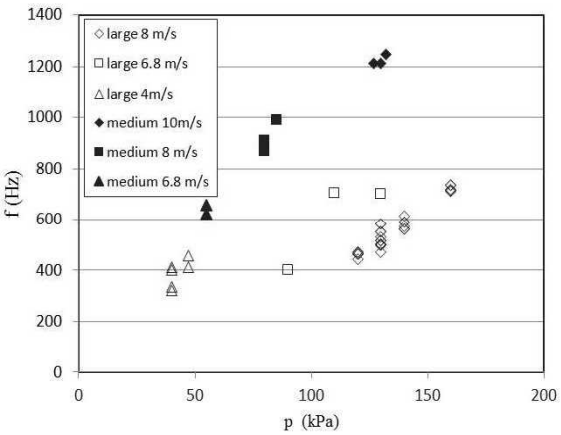

Fig. 8 Dominant frequency of the acoustic pulse as a function of test section static pressure